Vibrational Diagnostics of Rotating Stall in Centrifugal Compressors

by Donald E. Bently

Founder, Chairman, and CEO,
Bently Nevada Corporation, and
President,
Bently Rotor Dynamics
Research Corporation
e-mail: don@bently.com

and Paul Goldman

Manager,
Bently Rotor Dynamics
Research Corporation
e-mail: paul.goldman@bently.com

This paper discusses the rotating stall in centrifugal compressors from vibrational diagnostics and rotor dynamics standpoints. A diagnostic strategy is suggested from the overview of the case history and aerodynamic research. The literature survey shows insufficient understanding of rotor dynamic implications of the rotating stall. Most of the literature on the subject addresses only aerodynamic aspects of the problem, and only a few papers treat a compressor as a coupled mechanical-aerodynamic system. The latter approach is exercised in this paper. The results of the rotor/fluid system Dynamic Stiffness identification are presented for the experimental centrifugal compressor, in rotating stall and in normal operating conditions. It is shown that the aerodynamically-induced radial (direct spring) stiffness coefficients are negative in normal operating conditions. The negative spring effect in the case of rotating stall is even more profound. The conclusion is that during rotating stall the rotor dynamic stability margin is reduced.

Introduction

The interest in radial compressor fluid-induced instabilities started in the mid-seventies. Since then, numerous case histories of high pressure, centrifugal compressor instabilities have been published [1-17]. Most of the publications report two types of rotor vibrational behavior: 1) High eccentricity, rotor first natural frequency re-excitation; and 2) Subsynchronous forward precession with rotative-speed-dependent frequency. The former is usually referred to as whip-type behavior and is normally associated with balance pistons, fluid-film bearings, and labyrinth seals. The latter is called whirl-type behavior [27-28] and can be associated either with fluid-film bearings/seals or with rotating stall. Rotating stall usually results in an appearance of a low subsynchronous frequency component in the rotor vibration spectrum (frequency ratios are typically between 8 and 40% but can be as high as 80% of rotative speed, [20]). The emphasis on rotor behavior does not allow for details of particular flow patterns but treats the fluid (gas) "in average," which falls in the scale of rotor motion.

Experimental compressor

An experimental rig (Figure 1 and Table 1) was constructed to evaluate the rotor/fluid system Dynamic Stiffness during rotating stall and normal operating conditions. The rig consisted of a single stage, centrifugal

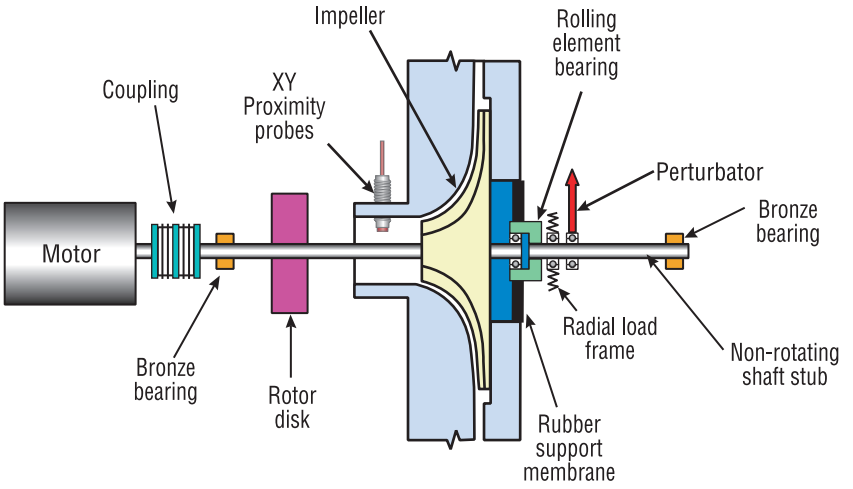

Figure 1. Experimental compressor.

Compressor type	Centrifugal, 1 stage, vaneless diffuser
Working fluid	Air at 84.1 kPa (12.2 psi), 20° C (68° F)
Number of impeller blades	11
Inlet diameter	51 mm (2 in)
Outside diameter of impeller	108 mm (4.3 in)
Diffuser/Impeller radius ratio	1.8
Impeller tip/Diffuser radial clearance	380 µm (0.015 in)
Impeller/Diffuser axial clearance	640 µm (0.025 in)
Diffuser/Shroud clearance	3 mm (0.12 in)
Discharge pipe dimensions	51 mm (2 in) inside diameter, 360 mm (14.2 in) length

Table 1. Compressor design and operating parameters.

compressor with a vaneless diffuser, driven by a 373 W (½ hp) dc electric motor. The motor speed was controlled by a high output, variable power supply, and the speed could be controlled from near zero to 17,000 rpm. The motor was attached to the compressor rotor by a flexible disk coupling.

The compressor rotor was separated into two pieces: a rotating section from the motor to the outboard end of the compressor, and a nonrotating stub shaft from the outboard compressor bearing to the outermost support bearing.

The rotating section was supported by two bearings: a bronze bushing type at the inboard (motor) end, and a rolling element bearing at the outboard end of the compressor. The outer race of the bearing was installed in a collar, which was attached to the nonrotating outboard stub shaft. This allowed free rotation of the compressor rotor relative to the nonrotating stub shaft. A flexible membrane made of stiff rubber supported the stub shaft collar and the bearing assembly. Another bronze bearing supported the outboard end of the nonrotating stub shaft.

An additional 0.8 kg (1.76 lb) disk was attached to the shaft between the inboard bearing and compressor to reduce the rotor system natural frequency.

An orthogonal pair of eddy current displacement transducers was mounted between the air inlet and the impeller to measure the displacement of the rotor.

A spring load frame was attached to the nonrotating stub shaft just outboard of the compressor. This was used to control the radial position of the compressor rotor and to counteract the gravity load of the rotor.

A conical exhaust valve on a lead screw controlled airflow through the compressor. The valve was located at the end of the discharge pipe from the compressor (Figure 2). It could be adjusted through several turns from fully closed, which completely blocked the output flow of the compressor, to fully open, which allowed free flow with minimum restriction. A pressure transducer measured the compressor discharge pressure.

A constant magnitude, rotating-force perturbator, used in modal testing, was attached to the nonrotating stub shaft. It transmitted an exciting rotating force with variable frequency to the compressor rotor. The perturbator consisted of an outer rotating assembly supported by a rolling element bearing attached to the compressor support structure. Three radial springs with 120° angular spacing were attached from the outer rotating assembly to an inner rolling element bearing attached to the nonrotating stub shaft. One of the springs was tensioned more than the other two springs, and this created a net force in the direction of the most tensioned spring. As the perturbator outer assembly rotated, the springs rotated as well, and a rotating force was created. The force was transmitted through the inner rolling element bearing to the stub shaft, and then to the compressor rotor. A variable speed motor drove the perturbator via a flexible belt. The perturbator drive motor was equipped with a Keyphasor® probe to supply a phase reference and speed indication. The magnitude of the

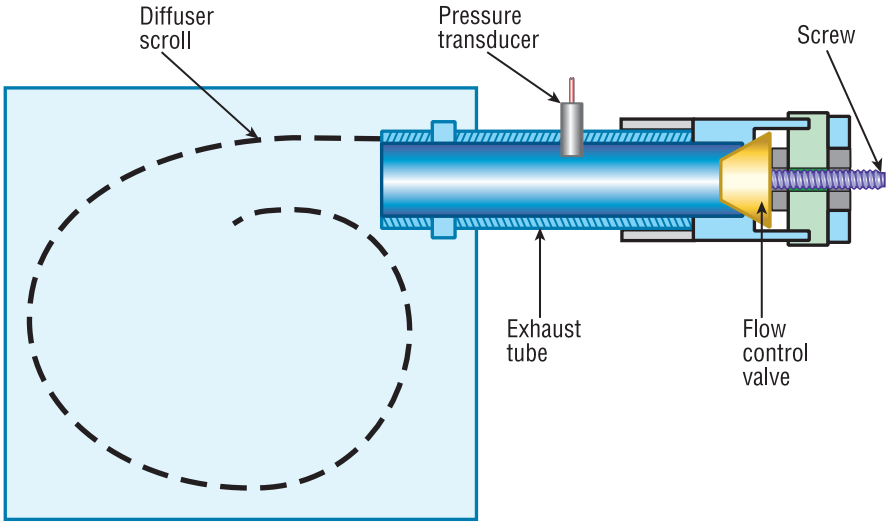

Figure 2. The experimental compressor discharge flow/pressure control.

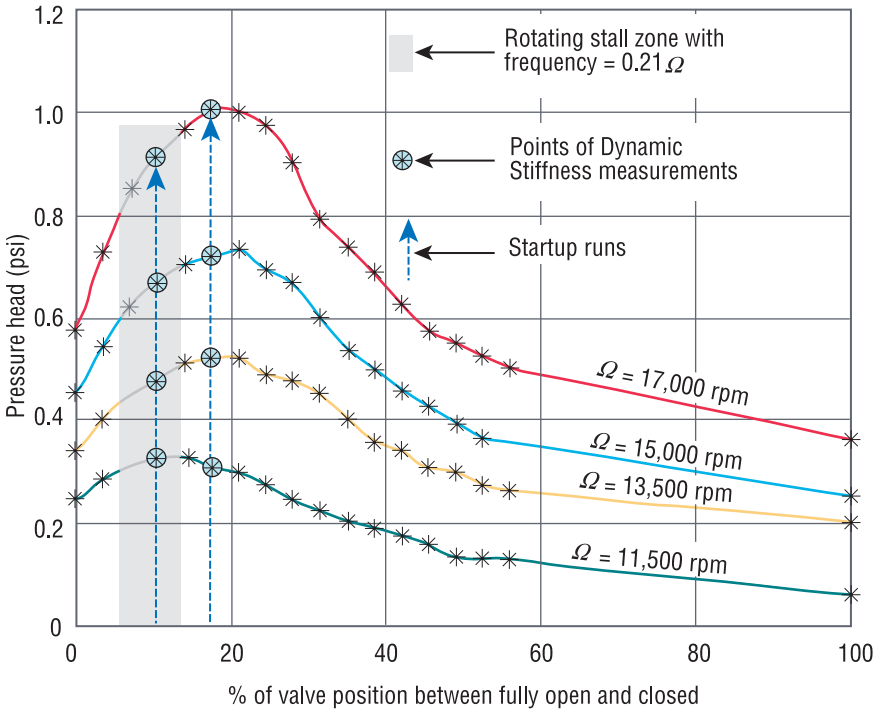

Figure 3. Experimental compressor performance chart. Ω = rotative speed.

rotating force, 1.3 N (0.3 lb), did not change noticeably with speed, and the perturbator provided a variable speed, constant magnitude, rotating-force excitation to the compressor rotor.

An experimental compressor performance chart is shown in Figure 3. It also depicts the points on the performance curves where the vibrational data was taken.

The first series of experiments consisted of compressor startups with two different discharge valve positions, while the perturbator was at rest. Valve positions, which were as close to each other as possible, were chosen to provide normal operating conditions and rotating stall conditions. During normal operation, predominantly 1X forward vibration was observed, with no subsynchronous vibration. The data is presented in the form of a 1X, forward component Bode plot and full spectrum cascade plot (Figure 4). The Bode plot shows the existence of two rotor modes in the range from 0 to 17,000 rpm. With the help of an additional set of probes, the first mode was identified as an almost rigid body conical mode of the shaft, while the second was a bending mode. The data taken during rotating stall is shown in Figure 5. Since the Bode plot of the 1X forward component in this case does not differ strongly from the previous experiment, only a typical orbit and full spectrum cascade are presented. The experimental compressor rotor exhibits rotating stall whirl with a subsynchronous frequency component of 0.21X in the forward direction. The subsynchronous component of the compressor rotor radial vibration is most likely caused by the diffuser rotating stall.

Rotor dynamic characteristics of rotating stall

The startup data does not provide sufficient information to identify any changes in the Dynamic Stiffness of the first mode due to rotating stall, because the mode occurs at rotative

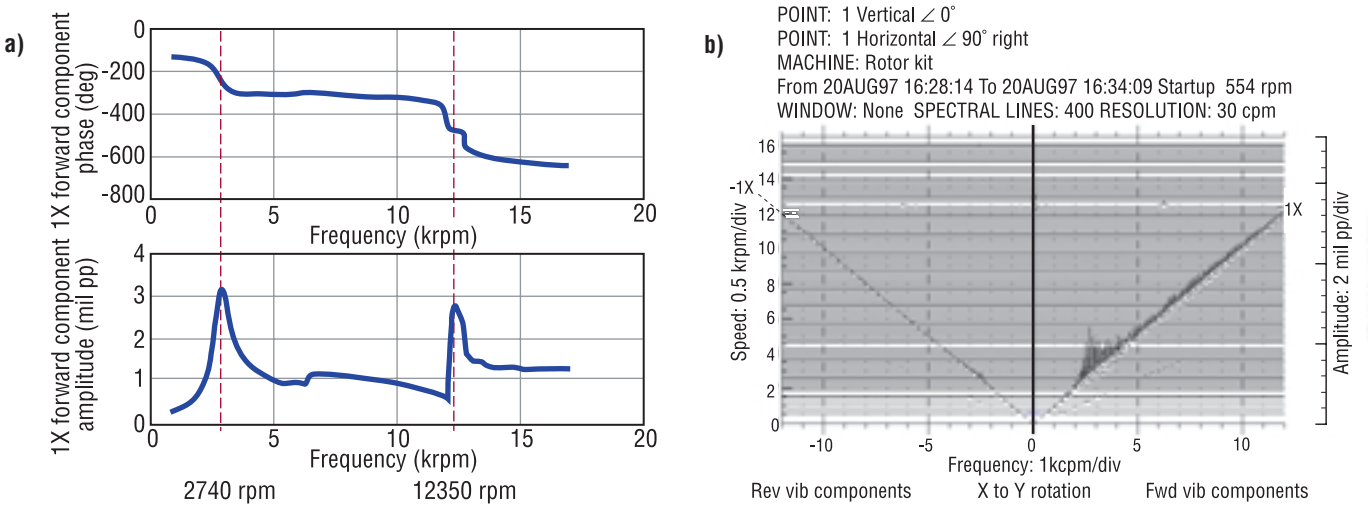

Figure 4. Rotor lateral X and Y vibration data of the experimental compressor during startup without rotating stall: a) 1X forward component Bode plot, b) Full spectrum cascade plot.

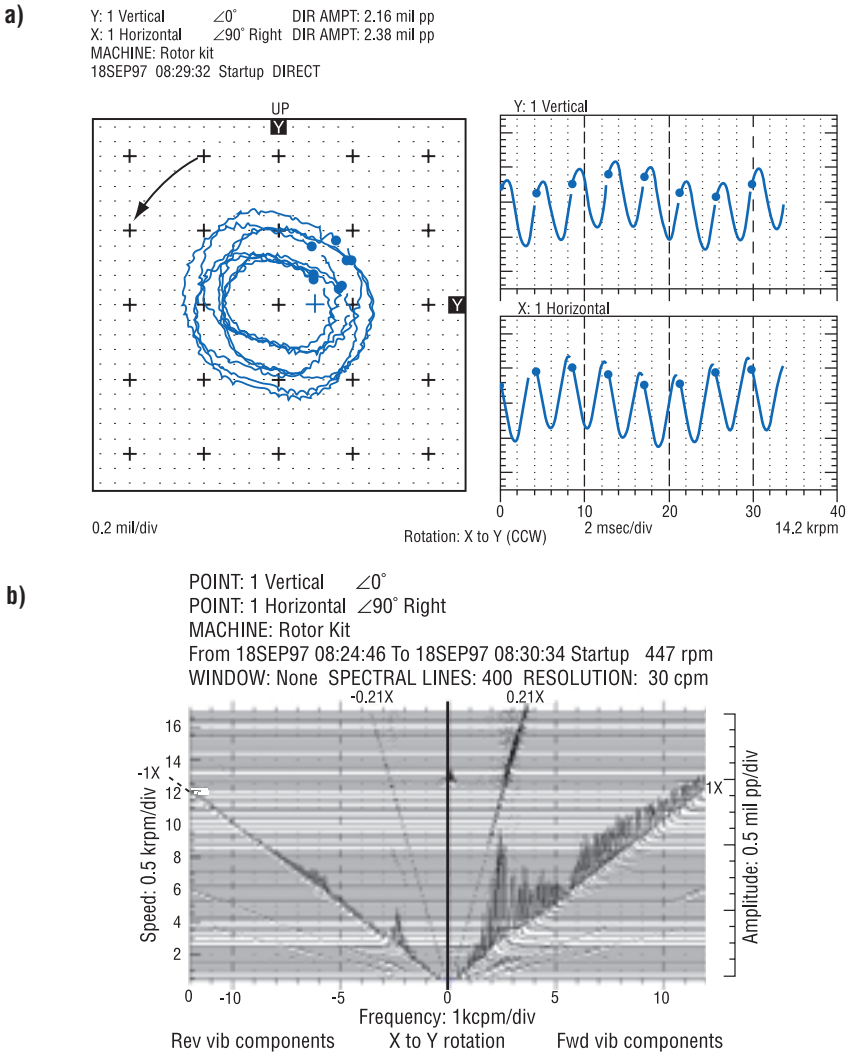

Figure 5. Rotor lateral X and Y vibration data of the experimental compressor rotor during startup with rotating stall: a) Typical orbit/timebase, b) Full spectrum cascade.

speed below the onset of rotating stall whirl. A series of nonsynchronous perturbation tests were performed at each of four compressor running speeds: 11,500; 13,500; 15,000; and 17,000 rpm. At each running speed, perturbation trials were performed for the two valve positions used in the startup tests. The constant force perturbator generates a force of magnitude F with orientation δ rotating in the same direction as the compressor rotation (forward perturbation), resulting in the perturbation vector $Fe^{j\delta}$. The perturbator was ramped up from slow roll speed to 3,000 rpm in order to identify Dynamic Stiffness of the rotor first mode. The vibration signals from two orthogonal eddy current displacement transducers, located at 90° to the right (X) and 0° (Y) relative to vertical (as seen from the driver), were filtered to the frequency ω of the perturbation force. This yielded amplitudes and phases for vertical and horizontal components of the response.

In order to eliminate the minor influence of mechanical stiffness asymmetry, 1X vertical $\vec{Y}_\omega$ and horizontal $\vec{X}_\omega$ vectors were combined into the circular component:

$$\vec{A}_\omega^{(fwd)} = \vec{Y}_\omega - j\vec{X}_\omega \qquad (1)$$

Next, the perturbation process was repeated for perturbation in a direction opposite the rotation of the compressor rotor (reverse perturbation) for each running speed Ω and valve setting. In this case, the forward (in the direction of perturbation) component of the filtered-to-perturbation-frequency response is opposite to the direction of rotation.

The nonsynchronous Dynamic Stiffness was calculated by taking the ratio of the force input to the response vectors for each speed in the databases.

$$DS(\omega) = \frac{Fe^{j\delta}}{\vec{A}_\omega^{(fwd)}} \qquad (2)$$

$$DDS(\omega) = direct(DS) \qquad (3)$$

$$QDS(\omega) = quad(DS) \qquad (4)$$

Since the total Dynamic Stiffness of the compressor consists of a mechanical and an aerodynamic part, the former was measured by running nonsynchronous perturbation on the compressor at zero rotative speed (DS_0). The difference between the Dynamic Stiffness of the running compressor and that of the stopped compressor represents aerodynamically-induced Dynamic Stiffness, DS_{air}:

$$DDS_{air}(\omega) = direct(DS - DS_0) \qquad (5)$$
$$= K_{air} - M_{air1}\omega^2 - 2M_{air2}\Omega\omega$$

$$QDS_{air}(\omega) = quad(DS - DS_0) \qquad (6)$$
$$= D_{air}\omega - T$$

where M_{air1}, K_{air}, and D_{air} are air inertia, radial stiffness, and damping, respectively, generated by the air/impeller interaction, M_{air2} is a fluidic mass term, and T represents a tangential force coefficient.

Equations 5 and 6 show the parameters of Direct and Quadrature Stiffness extrapolation, that fit the data within an accuracy of about 2% compared to actual.

The raw data and the described data processing is illustrated in Figure 6. The results of all perturbation tests, reduced to the parameters of air-induced Dynamic Stiffness (Equations 5 and 6), are presented in Table 2.

The most significant conclusion from the results in Table 2 is that aerodynamic forces applied to the impeller generate negative spring stiffness (damping D_{air} and stiffness K_{air} appear negative in all experiments). It is also important that this stiffness drops even more during the rotating stall. This result is also shown in Figure 7. Inconsistency in tangential force coefficient T suggests that it was too small in the experiment and was not determined with sufficient accuracy.

Case history

A 5-stage propylene compressor provides an example of the industrial centrifugal compressor behavior under the conditions of surge/rotating stall. The orbit (Figure 8) shows a typical forward precession with frequency 0.15X. This is supported by the lateral vibration, half spectrum cascade data (Figure 9). The gas pressure measured at the outlet of the third stage is presented in the timebase waveform for the steady state regime (Figure 10) and half spectrum cascade plot for the startup (Figure 11). The steady state data shows the combination of vane passing high frequency with low frequency pulsations. Using the half spectrum cascade plot, the latter are identified as a surge component (3.5 Hz) and rotating stall component (0.15X). It is important to note that the half spectrum cascade of the thrust probe data (Figure 12) shows a strong activity at the surge frequency, while the rotating stall component is much smaller. The described behavior is a reflection of the surge, which propagates axially, while rotating stall is mainly active in the circumferential direction.

Instrumentation and diagnostics strategy

A typical machine train for a centrifugal compressor unit is shown in Figure 13. It includes an engine (in this case an aeroderivative gas turbine), gearbox, and the compressor itself. Different instrumentation configurations for vibration, as well as performance diagnostics and monitoring of the engine, are beyond the scope of this paper. For the centrifugal compressor, the instrumentation package normally includes a Keyphasor® transducer, two sets of proximity probes in XY configuration installed at the inboard and outboard bearing locations (see Compressor DE and Compressor NDE in Figure 13), two axial transducers, and performance monitoring

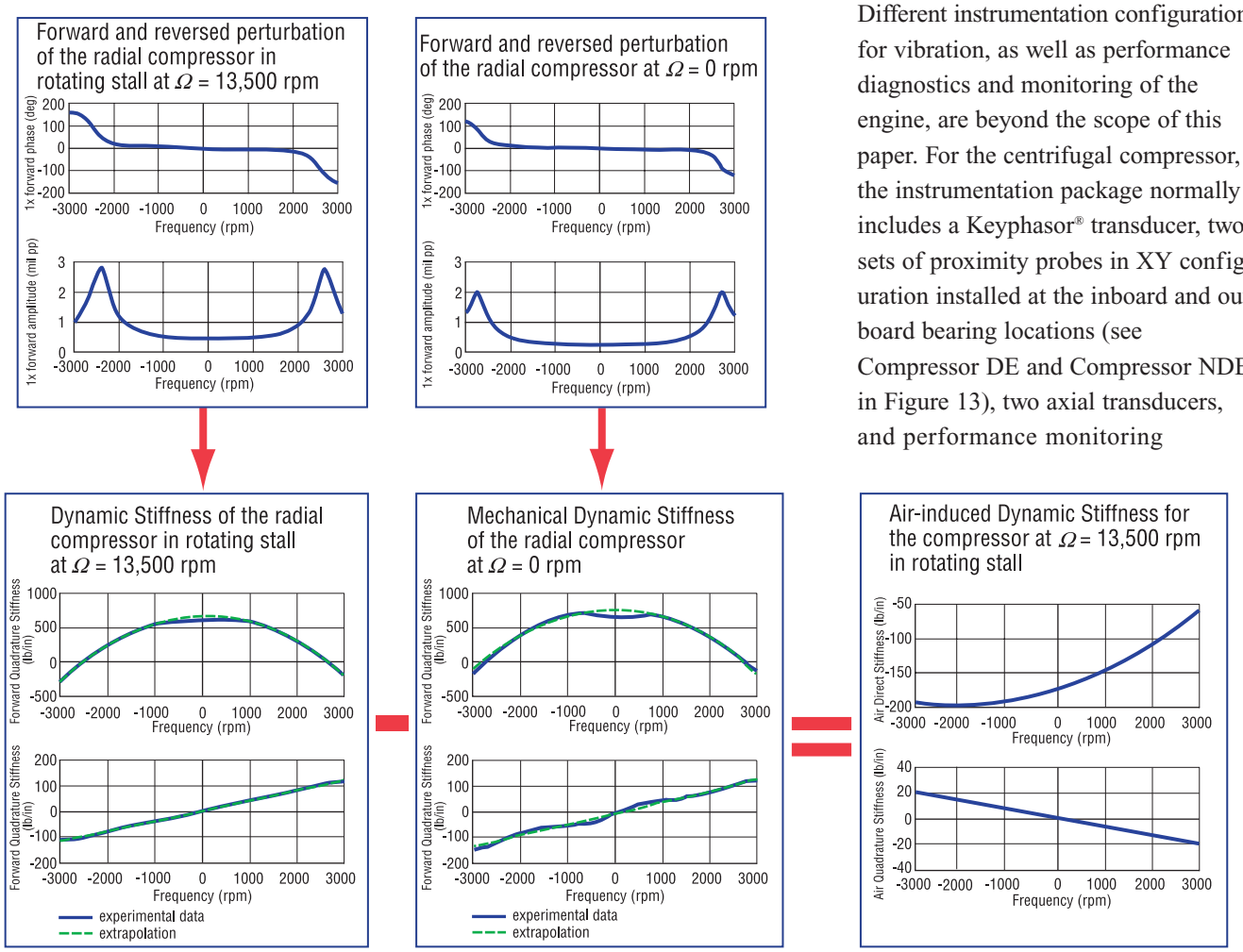

Figure 6. Identification of the air-induced Dynamic Stiffness component.

Rotative speed	Parameters		No rotating stall	With rotating stall	Stiffness change, %, relative to normal conditions
11,500 rpm	K_{air}	lb/in	-52.16	-63.2	-21
	D_{air}	lb•s/in	-3.4×10^{-3}	-3.0×10^{-3}	
	M_{air1}	lb•s²/in	-2.7×10^{-6}	-3.0×10^{-6}	
	M_{air2}	lb•s²/in	-9.75×10^{-6}	-9.7×10^{-6}	
	T	lb/in	2.83	3.6	
13,500 rpm	K_{air}	lb/in	-134.6	-186.4	-38
	D_{air}	lb•s/in	-7.0×10^{-3}	-8.3×10^{-3}	
	M_{air1}	lb•s²/in	-4.3×10^{-6}	-7.7×10^{-6}	
	M_{air2}	lb•s²/in	-10.0×10^{-6}	-7.7×10^{-6}	
	T	lb/in	-0.52	-0.07	
15,000 rpm	K_{air}	lb/in	-66.7	-134.1	-101
	D_{air}	lb•s/in	-5.7×10^{-3}	-5.7×10^{-3}	
	M_{air1}	lb•s²/in	-4.3×10^{-6}	-4.3×10^{-6}	
	M_{air2}	lb•s²/in	-10.0×10^{-6}	-10.0×10^{-6}	
	T	lb/in	-0.52	-0.52	
17,000 rpm	K_{air}	lb/in	-63.2	-130.8	-107
	D_{air}	lb•s/in	-5.2×10^{-3}	-6.4×10^{-3}	
	M_{air1}	lb•s²/in	-1.5×10^{-6}	-5.0×10^{-6}	
	M_{air2}	lb•s²/in	-8.7×10^{-6}	-8.3×10^{-6}	
	T	lb/in	3.6	2.7	

Table 2. Parameters of the aerodynamically-induced Dynamic Stiffness.

instrumentation. As a minimum, the compressor performance monitoring instrumentation is supposed to include inlet and discharge pressures and temperatures, and discharge flow measurements. Using the described instrumentation, the rotating stall or surge can be identified based on the following information:

- **Radial vibration**

  Steady state data: direct orbits, full spectrum

  Indication: subsynchronous forward component

  Possible causes: **rotating stall**, fluid-induced instability, and surge

  Transient data: direct orbits, full spectrum cascade

  Indication: subsynchronous forward component with frequency proportional to the rotative speed (0.1 to 0.8X)

  Possible causes: **rotating stall**, fluid-induced instability

- **Axial vibration**

  Steady state data: spectrum

  Indication: subsynchronous component

  Possible causes: **rotating stall** (possible weak coupling), and surge

  Transient data: spectrum cascade

  Indication: subsynchronous component with low constant frequency

  Possible cause: **surge**

- **Pressure, temperature, flow**

  Trend data (dc signal)

  Indication: pressure, head, and flow decrease, temperature increase

  Possible causes: **surge**, less likely rotating stall

  Note: if pressure head and flow indicate a position on the performance curve close to the surge point, it could support rotating stall or surge versus fluid-induced instability

  Dynamic data

  Indication: vane passing frequency amplitude modulation of pressure, with constant flow

  Possible cause: **rotating stall**

  Indication: pressure vane passing frequency amplitude modulation with correlated flow oscillations

  Possible cause: **surge**

As indicated above, a strong conclusion can only be reached by the correlation of vibration data with performance information. It is important to note that rotating stall can originate in a particular stage of a multistage compressor. To localize the rotating stall source, additional pressure transducers may be required.

Conclusions

Although, the rotating stall aerodynamic effects have been investigated extensively [16-23], the rotor dynamic implications of this phenomenon have received much less attention [24, 27-29]. A direct quotation from the paper [26] by Colding-Jorgensen serves as an example of insufficiency of rotor dynamic data:

"In spite of all reservations due to difficulties and lack of data, it is the author's opinion that the impeller-casing effect is mainly responsible for a negative direct stiffness effect."

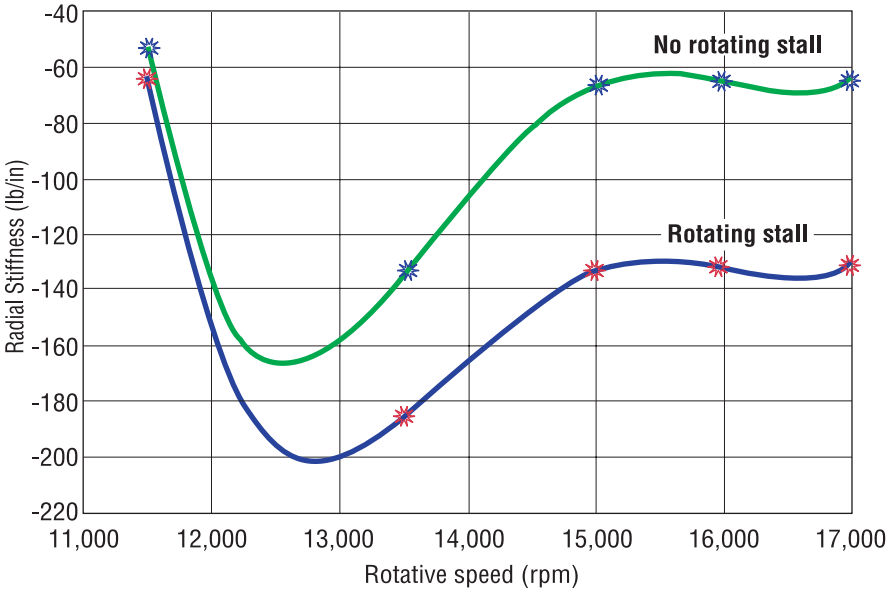

Figure 7. Aerodynamically-induced radial stiffness of experimental compressor.

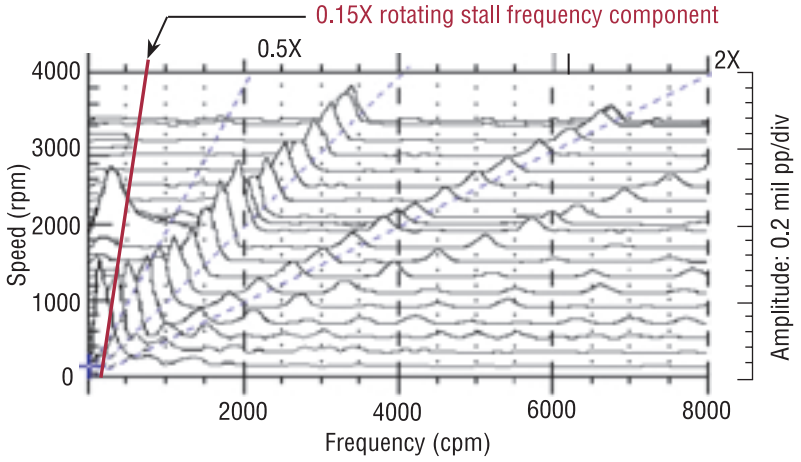

Figure 9. Half spectrum cascade plot of the vertical inboard lateral vibrations of the rotor at the outboard bearing of the 5-stage propylene compressor during startup.

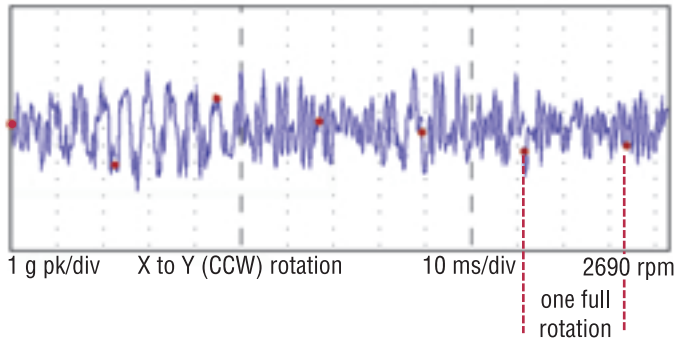

Figure 10. Gas pressure oscillations measured at the outlet of the third stage of 5-stage propylene compressor in steady state regime. Note high vane passing frequency modulated by the low frequency of rotating stall/surge.

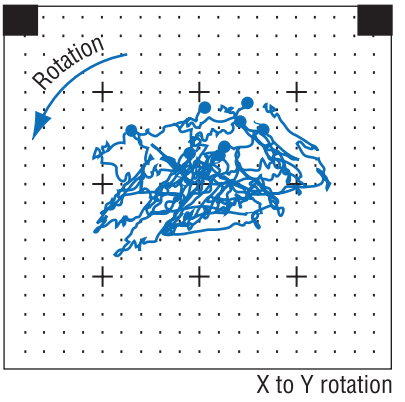

Figure 8. Typical orbit of a 5-stage propylene centrifugal compressor rotor in rotating stall conditions.

This paper provides some practical recommendations on the rotating stall diagnostics as well as some insight into rotor dynamic implications of the phenomenon. In short, the conclusions can be formulated as follows:

- The rotating stall conditions manifest in the rotor vibration signature as rotor forward precession with subsynchronous frequency, which tracks the rotor speed. This behavior is referred to as a rotating stall whirl.
- From the diagnostic standpoint, rotating stall differs from the other instabilities of the whirl type in its strong dependence on the compressor operating conditions; it should disappear with increased flow. It differs from surge by its frequency proportionality to the rotative speed as well as by the predominantly axial character of surge-caused vibrations.
- The parameter clearly identified by nonsynchronous perturbation tests is aerodynamically-induced direct spring stiffness. In all conditions it was negative. From the practical standpoint, it means that even in normal operating conditions, centrifugal compressors

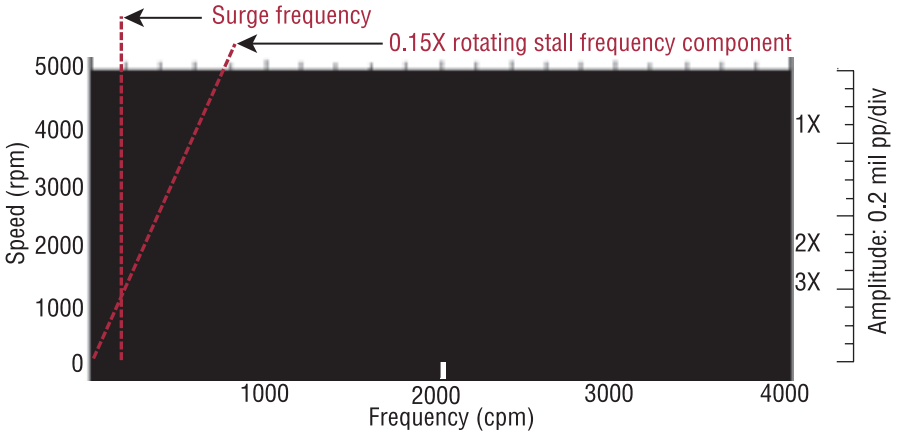

Figure 11. Half spectrum cascade plot of gas pressure oscillations at the outlet of the third stage of 5-stage propylene compressor during startup.

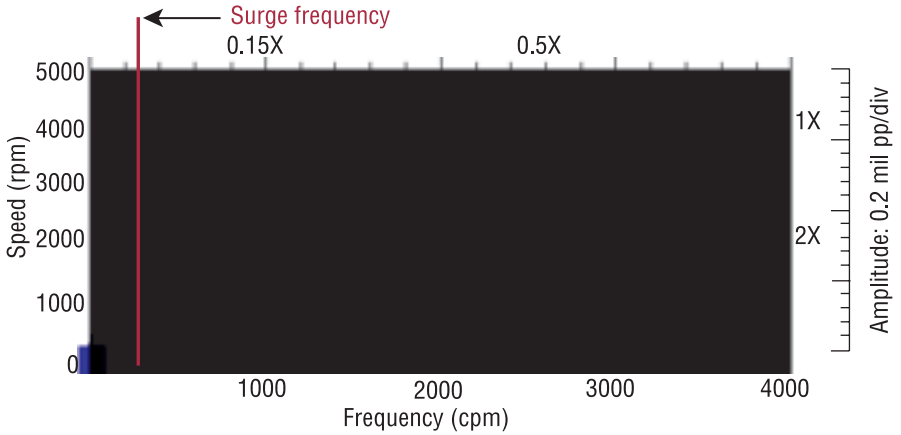

Figure 12. Half spectrum cascade plot of the rotor axial vibrations of the 5-stage propylene compressor during startup, showing surge component.

have lower natural frequencies than follows from purely mechanical calculations.

- The aerodynamically-induced Direct Stiffness during rotating stall drops dramatically and ultimately can make a compressor unstable.
- Altogether, aerodynamic forces may have a significant destabilizing effect on the compressor. In the case of a flexible rotor and/or soft bearings, they are able to create a rotor dynamic instability of whirl type.

References

1. Fowlie, D. W., Miles, D. D., "Vibration Problems With High Pressure Centrifugal Compressors," *ASME Paper 75-Pet-28, Petroleum Mechanical Engrg. Conf.*, Tulsa, Oklahoma, 1975.
2. Smith, K. J., "An Operation History of Fractional Frequency Whirl," *Proceedings of Fourth Turbomachinery Symposium*, 1975.
3. Wachel, J. C., "Nonsynchronous Instability of Centrifugal Compressors," *ASME Paper 75-Pet-22, Petroleum Mechanical Engrg. Conf.*, Tulsa, Oklahoma, 1975.
4. Ferrara, P., "Vibrations in Very High Pressure Centrifugal Compressors," *ASME Paper 77-Det-15, Design Engrg. Technical Conf.*, Chicago, Illinois, 1977.

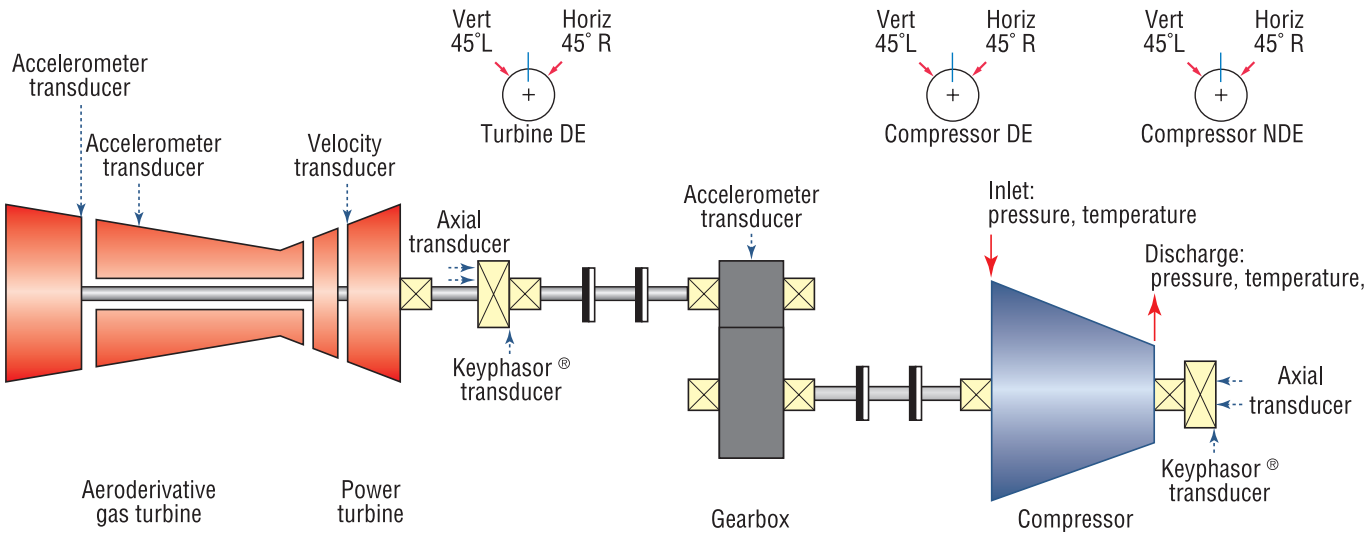

Figure 13. Typical compressor train diagram.

5. Kaneki, T., Eino, T., "Centrifugal Carbon Dioxide Compressor for Urea Synthesis Plant," *Hitachi Review, Vol. 28, No. 6*, 1979.
6. Ek, M. C., "Solution of the Subsynchronous Whirl Problem in the High Pressure Hydrogen Turbomachinery of the Space Shuttle Main Engine," *AIAA/SAE 14th Joint Propulsion Conference*, Las Vegas, Nevada, 1978.
7. Geary, C. H., Damratowsky, L. P., Seyer, C., "Design and Operation of the World's Highest Pressure Gas Injection Centrifugal Compressor," *No. 0TC 2485, Offshore Technology Conference*, Houston, Texas, 1976.
8. Sabella, D., Terrinoni, L., Timori, A., "Full Load Testing of Centrifugal Natural Gas Injection Compressors," *Inst. Mech. Ing. Conference Publications*, March 3, 1981.
9. Coletti, N. J., Crane, M. E., "Centrifugal Compression on the Arun High Pressure Injection Project," *Inst. Mech. Ing. Conference Publications*, March 3, 1981.
10. Bonciani, L., Ferrara, P. L., Timori, A., "Aero-Induced Vibrations in Centrifugal Compressors," *Workshop on Rotordynamic Instability* at Texas A&M University, College Station, Texas, 1980.
11. Bonciani, L., Terrinoni, L., Tesei, A., "Unsteady Flow Phenomena in Industrial Compressor Stage," *NASA Conference Publication 2250*, 1982.
12. Excerpts From Turbomachinery Technology Seminar, March 11-14, 1984, Coronado, California.
13. Wendt, P. G., "Forced Low Frequency Vibration Due to Aerodynamic Flow Instability (Rotating Stall)," *Solar Turbines, Inc., Engineering Report 2832*, January 23, 1985.
14. Fulton, J. W., "Subsynchronous Vibration of a Multistage Centrifugal Compressor Forced by Rotating Stall," *Turbomachinery Technology Seminar 1986*, Solar Turbines, Inc., San Diego, California, February 1986.
15. Emmons, H. W., Pearson, C. E., Grant, H. P., "Compressor Surge and Stall Propagation," Trans. *ASME, Vol. 79*, 1955.
16. Lennemann, E., Howard, J. H. G., "Unsteady Flow Phenomena in Rotating Centrifugal Impeller Passages," *ASME 69-GT-35, ASME Journal of Engrg. for Power, Vol. 108*, 1970.
17. Frigne, P., Van den Braembusse, R., "Distinction Between Different Types of Impeller and Diffuser Rotating Stall in a Centrifugal Compressor With Vaneless Diffuser," *ASME Journal of Engrg. for Gas Turbines and Power, Vol. 106, No. 2*, 1984.
18. Van den Braembusse, R., "Rotating Stall in Centrifugal Compressors," *von Karman Institute for Fluid Dynamics, Preprint 1987-16*, March 1987, Belgium.
19. Haupt, U., Seidel, U., Abdel-Hamid, A. N., Rautenberg, M., "Unsteady Flow in a Centrifugal Compressor With Different Types of Vaned Diffusers," *ASME Paper 88-GT-22, Gas Turbine and Aeroengine Congress and Exposition*, Amsterdam, The Netherlands, 1988.
20. Jin, D., Haupt, U., Hasemann, H., Rautenberg, M., "Blade Excitation by Circumferentially Asymmetric Rotating Stall in Centrifugal Compressors," *ASME Paper 92-GT-148*.
21. Chen, J., Huang, X., Hasemann, H., Seidel, U., Jin, D., Rautenberg, M., "The Interpretation of Internal Pressure Patterns of Rotating Stall in Centrifugal Compressor Impellers," *ASME Paper 93-GT-192*.
22. Tsujimoto, Y., Acosta, A. J., "Theoretical Study of Impeller and/or Vaneless Diffuser Attributed Rotating Stalls and Their Effects on Whirling Instability of a Centrifugal Impeller," *Work Group of Hydraulic Machinery Under Steady Oscillatory Conditions*, Lille, France, 1987.
23. Pampreen, R. C., "Compressor Surge and Stall," *Concepts ETI, Inc.*, Norwich, Vermont, 1993.
24. Bently, D. E., Muszynska, A., "Role of Circumferential Flow in the Stability of Fluid-Handling Machine Rotors," *The Fifth Workshop on Rotordynamic Instability Problems in High Performance Turbomachinery*, Texas A&M University, College Station, Texas, NASA CP 3026, 1988.
25. Muszynska, A., Bently, D. E., "Frequency Swept Rotating Input Perturbation Techniques and Identification of the Fluid Force Models in Rotor/Bearing/Seal Systems and Fluid-Handling Machines," *Journal of Sound and Vibration, Vol. 143, No. 1*, 1990.
26. Colding-Jorgensen, J., "Rotordynamic Effects of Impeller Flow in Centrifugal Compressors," *VDI Bevichte, No. 1082*, 1993.
27. Bently, D. E., Goldman, P., "Destabilizing Effect of Aerodynamic Forces in Centrifugal Compressors," *ISROMAC-7*, Honolulu, Hawaii, February 1998.
28. Sorokes, J. M., Marshall D. F., "A Review of Aerodynamically Induced Forces Acting on Centrifugal Compressors, and Resulting Vibration Characteristics of Rotors," *Proceedings of the 27th Turbomachinery Symposium*, Texas A&M, September 1998.

ANNOUNCEMENT

Bently Rotor Dynamics Research Corporation Appoints New Manager

Paul Goldman, Ph.D., was promoted to Bently Rotor Dynamics Research Corporation (BRDRC) Manager on 15 December 1999. He had been Acting Research Manager for six months prior to his promotion, and, before that, he was a Senior Research Scientist. Paul's new responsibilities include providing major research directions, visions, and plans for BRDRC.

A native of St. Petersburg, Russia, Paul joined BRDRC in 1990. He earned an M.S.M.E. and Ph.D. in Applied Mathematics from State Technical University of St. Petersburg. He has conducted research in rotating machinery dynamics-related topics, including loose pedestal effect, rotor-to-stator rubbing, lateral/torsional cross-coupling, fluid dynamics of oil film bearings, rotating stall, and cracked shaft. He has authored or co-authored over 45 technical papers and reports.